Kent Academic Repository

Netherwood, Daniel J., Tam, Alexander K. Y., Gourlay, Campbell W., Knežević, Tea, Gardner, Jennifer M., Jiranek, Vladimir, Binder, Benjamin J. and Green, J. Edward F. (2025) *Accidental and Regulated Cell Death in Yeast Colony Biofilms.* Bulletin of Mathematical Biology, 87 (8). ISSN 0092-8240.

Society for
Mathematical
Biology

ORIGINAL ARTICLE

Check for
updates

Accidental and Regulated Cell Death in Yeast Colony Biofilms

Daniel J. Netherwood[1] · Alexander K. Y. Tam[2] · Campbell W. Gourlay[3] ·
Tea Knežević[4] · Jennifer M. Gardner[4] · Vladimir Jiranek[5] ·
Benjamin J. Binder[1] · J. Edward F. Green[1]

Abstract

The yeast species *Saccharomyces cerevisiae* is one of the most intensively studied organisms on the planet due to it being an excellent eukaryotic model organism in molecular and cell biology. In this work, we investigate the growth and morphology of yeast colony biofilms, where proliferating yeast cells reside within a self-produced extracellular matrix. This research area has garnered significant scientific interest due to its applicability in the biological and biomedical sectors. A central feature of yeast colony biofilm expansion is cellular demise, which is onset by one of two independent mechanisms: either accidental cell death (ACD) or regulated cell death (RCD). In this article, we generalise a continuum model for the nutrient-limited growth of a yeast colony biofilm to include the effects of ACD and RCD. This new model involves a system of four coupled nonlinear reaction–diffusion equations for the yeast-cell density, the nutrient concentration, and two species of dead cells. Numerical solutions of the spatially one and two-dimensional governing equations reveal the impact that ACD and RCD have on expansion speed, morphology and cell distribution within the colony biofilm. Our results are in good qualitative agreement with our own experiments.

1 Introduction

We investigate how two nutrient-dependent cell death mechanisms affect the expansion speed, morphology, and cell distribution of yeast colony biofilms. Biofilms are communities of microorganisms that reside within a self-produced extracellular matrix (ECM) (Costerton et al. 1999), which itself is adhered to a surface. The ECM protects the biofilm from external insults (Beauvais et al. 2009; Flemming and Wingender 2010) and facilitates efficient transportation of nutrients and water (Váchová et al. 2011). More than 80% of all microbial life is found within biofilms (Martinez and

Extended author information available on the last page of the article

Springer

Fries 2010), making them one of the most prevalent life forms on Earth (Flemming and Wingender 2010). Biofilms impact human life in several ways. Positive impacts include: wastewater treatment, food preservation, and other areas of biotechnology. However, the main impact of biofilms is their role in pathogenic bacterial and fungal infections (Martinez and Fries 2010). Biofilms are known to colonise medical devices, and are a leading cause of hospital-acquired infections. Yeast biofilms of *Candida albicans* yeasts (Pentland et al. 2021) cause invasive candidiasis, a disease responsible for approximately 20% of bloodstream infections in intensive-care units (Pappas et al. 2018). These major impacts, together with the rise of antimicrobial resistance, motivate the continued research into the mechanisms that promote and inhibit biofilm expansion.

In this work, we consider colony biofilms formed by the yeast species *Saccharomyces cerevisiae*, which is canonically referred to as the baker's yeast. *S. cerevisiae* is a major model organism in biofilm research (Reynolds and Fink 2001; Reynolds et al. 2008; Andersen et al. 2014; Bojsen et al. 2012), and was the first eukaryote to have its genome sequenced (Goffeau et al. 1996). Soon after, Reynolds and Fink (2001) demonstrated that *S. cerevisiae* can form colony biofilms on semi-solid agar. These colonies are single-species structures consisting of cells and ECM. They represent an experimental model for the formation of more complicated multi-species yeast biofilms found in medical and industrial settings (Tek et al. 2018; Tam et al. 2018). Throughout this work, we use the terms colony biofilms or colonies to describe these single-species entities, in accordance with Plocek et al. (2020).

Yeast species can alter their growth in response to their environment. For example, on the microscopic scale, individual yeast cells are thought to forage or move away from the colony by elongating, a process that creates filamentous patterns (Gimeno et al. 1992). On the macroscale, entire colonies are known to develop nutrient-driven spatiotemporal instabilities, leading to floral morphologies (Chen et al. 2014; Tam et al. 2018). In this work, we investigate how cell death affects the growth and dynamics of colony biofilms. Figure 1 illustrates three examples of *S. cerevisiae* colony biofilm growth from our own experiments.

In each experiment, the yeast colony is stained with a water-soluble red dye, Phloxine B (Middelhoven et al. 1976; Cannon et al. 1986; Peck et al. 1997; Leadsham et al. 2009). An increased intensity of red colour in each photograph is indicative of regions within the colony where membrane permeability has been compromised due to a sufficient drop in metabolism, which is a strong indication of cell death (Leadsham et al. 2010). In Figure 1A, there is a large circular region of cell death in the centre of the colony, surrounded by mostly living cells close to the leading edge. This pattern resembles that of a necrotic core observed in spheroidal tumour growth (Greenspan 1972; Byrne and Chaplain 1996; Byrne et al. 2003). In Figure 1B, the colony expands axisymmetrically, having a distinct red ring of cell death trailing the leading edge. There is also a region of elevated cell death near the centre of the colony, albeit not as pronounced as the ring or in the core of Figure 1A. Figure 1C shows a colony biofilm grown in a rectangular Petri dish, which also shows a stripe of dead cells trailing the edge of the colony. The colony in Figure 1C was initiated as a thin stripe of cells in the centre. During the expansion, the colony develops a spatially non-uniform front shape, similar to the petal formation in circular experiments reported by (Tam
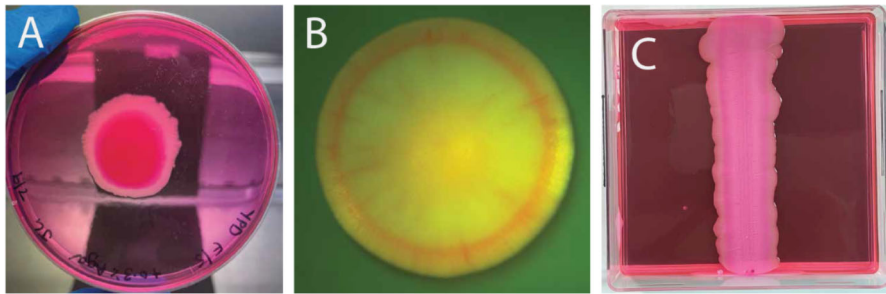
Fig. 1 Three experimental photographs of yeast colony biofilm formation. Dark pink/red regions in each photograph show regions where yeast cells have taken up Phloxine B dye, indicating regions of cell death. The experimental method is described in Section 2.2. (A) *Magnusiomyces magnusii* colony biofilm grown from a small spot inoculation at the centre of a circular Petri dish (10 days), with cell death occurring in the centre of the colony. (B) *S. cerevisiae* colony biofilm grown on agar (5 days). (C) *S. cerevisiae* colony biofilm grown from an inoculum streaked from top to bottom of a rectangular Petri dish filled with 0.9% YPD agar (19 days), with a stripe of death trailing the expanding edge, and an unstable front pattern

et al. 2018). Here, we investigate how nutrient limitation and cell death influence the different cell-death patterns and colony morphologies observed in Figure 1.

The review by Carmona-Gutierrez et al. (2018) summarises the current research in yeast-cell death, highlighting two specific mechanisms of cellular demise, namely Accidental Cell Death (ACD) and Regulated Cell Death (RCD). ACD occurs when cells encounter harsh and unpredictable environments, such as insufficient nutrient supplies (Gourlay et al. 2006). This cell-death mechanism results in a necrotic cell morphotype, whereby cells experience structural disintegration and uncontrolled rupturing of the plasma membrane. On the other hand, RCD is cellular suicide designed to benefit the survival of the colony as a whole. RCD typically occurs in response to mild stresses, though it can be entirely initiated by the cell. RCD yields a spectrum of cell-death morphotypes. An important hypothesis is that both ACD and RCD can release nutrients back to the surrounding environment for further consumption by the cells (Čáp et al. 2012; Váchová and Palková 2005) and it is expected that RCD does so more efficiently and at a faster rate than ACD. RCD is therefore expected to have a more positive impact on the colony by producing a larger additional nutrient supply, promoting growth. It is noted that the dead matter that is not resupplied to the colony in the form of nutrient is inert biomass Laspidou and Rittmann (2002, 2004).

Whilst there have been recent advancements in measuring the lifespan of a cell (Minois et al. 2005; Werner-Washburne et al. 1996), obtaining an explicit diagnosis of cell death remains an experimental challenge. This is because a diagnosis of cell death can be made only when irreversible breakdown of the plasma membrane or complete cellular fragmentation is detected (Carmona-Gutierrez et al. 2018). The vitality dye Phloxine B used in our experiments is only retained in metabolically inactive cells that cannot expel the dye. Whilst this is a reliable indication of cell death, it does not explicitly measure death, nor the mechanism by which the cell may have died. For this reason, we turn to mathematical modelling for further insight. Scientists have used agent-based (Tronnolone et al. 2018; Li et al. 2024; Picioreanu et al. 1998), hybrid (Ghosh and Levine 2017), reaction–diffusion (Tam et al. 2018; Chen

et al. 2014; Müller and van Saarloos 2002; Gallegos et al. 2006; Gray and Kirwan 1974; Kawasaki et al. 1997; Giverso et al. 2015), and mechanical (Tam et al. 2019, 2022; Ward and King 2012; Dockery and Klapper 2001; Eberl et al. 2001; Lega and Passot 2003; Clarelli et al. 2015; Wanner and Gujer 1986) mathematical models to study biofilm formation and growth (Mattei et al. 2018; Klapper and Dockery 2010). Work has been done to incorporate cell death into some of these models (Kitsunezaki 1997; Ghosh and Levine 2017; Asally et al. 2012). Ghosh and Levine (2017) used an agent-based model and reaction–diffusion system with a Heaviside step function in the reaction term to show that nutrient-limited cell death (an instance of ACD) and cell death occurring randomly throughout the colony both amplify front patterns. Whilst clear progress has been made to improve our understanding of the impact that cell death has on colony biofilm expansion, comparatively little is understood about the effect that the mechanisms of ACD and RCD, and their breakdown and subsequent nutrient release have on growth dynamics.

Here, we develop a continuum reaction–diffusion model incorporating nutrient limitation, ACD, and RCD, as well as cellular breakdown and nutrient release. We neglect mechanical effects and the ECM, and start from a system of nonlinear reaction–diffusion equations for nutrient-limited growth considered by several authors (Tam et al. 2018; Müller and van Saarloos 2002; Chen et al. 2014), and modify the model to incorporate cell death. This original model investigates a colony biofilm occupying a fixed Petri dish, and involves the following system of reaction–diffusion equations:

$$\frac{\partial n^*}{\partial t^*} = D_n^* \nabla \cdot \left(n^* \nabla n^*\right) + \alpha^* n^* g^*, \tag{1.1a}$$

$$\frac{\partial g^*}{\partial t^*} = D_g^* \nabla^2 g^* - c^* \alpha^* n^* g^*, \tag{1.1b}$$

where $n^*(\boldsymbol{x}, t)$ and $g^*(\boldsymbol{x}, t)$ are the dimensional living-cell density and nutrient concentration at dimensional time t^* and dimensional position $\boldsymbol{x}^*$, and ∇ is the spatially two-dimensional gradient operator. Since yeast-cell diffusion occurs more rapidly in regions of elevated cell density, living-cell diffusion is inherently nonlinear (Müller and van Saarloos 2002). We therefore adopt the nonlinear degenerative diffusion law used previously by Müller and van Saarloos (2002) and later by Tam et al. (2018), where D_n^* is the dimensional living-cell diffusivity constant. In this model, nutrients are assumed to diffuse according to Fick's law with dimensional diffusivity D_g^*. The colony expands through cell proliferation, facilitated by nutrient consumption. The constant α^* is the dimensional rate of cell proliferation, and c^* is a dimensional constant indicating the amount of nutrient required to produce a new cell.

A common technique applied to reaction–diffusion systems such as (1.1) is to analyse the spatiotemporal stability of transversely-perturbed travelling-wave solutions (Oelker 2017; Yang et al. 2002; Sivashinsky 1977; Hilhorst et al. 2008; Horváth et al. 1993). As demonstrated by Tam et al. (2018) and others, when equipped with appropriate boundary and initial conditions, the minimal reaction—diffusion model (1.1) can be used to predict the expansion speed and front patterns of yeast

colony biofilms in the absence of cell death. In this article, we introduce ACD and RCD into (1.1) under the assumption that their onset mechanisms (starvation, *etc.*) are exclusively nutrient dependent and investigate numerically their influence on the systems evolution into a non-uniform front shape.

The remainder of the paper is organised as follows. In Section 2, we present the mathematical model and experimental method. We use a four-species reaction–diffusion system for yeast-cell density, nutrient distribution, and the density of cells having undergone either ACD or RCD. We assume that ACD occurs when the nutrient concentration drops below a prescribed threshold, and that RCD occurs in a prescribed window of nutrient concentration. In Section 3.1, we show that our model is capable of producing the patterning observed in Figure 1. In Section 3.2, we demonstrate qualitatively that cell death in isolation amplifies the instability of a planar front, causing a more pronounced petal formation, and in Section 3.2.2 we show that such an instability no longer occurs if nonlinear diffusion is replaced with linear diffusion. Our results indicate that RCD can offer a survival advantage to the colony. RCD with nutrient recovery increases expansion speed compared to the scenario with death but no nutrient recovery, and helps petals to invade nutrient-rich regions of the Petri dish. ACD or excessive RCD can inhibit growth, suggesting a balance between the altruistic and destructive effects of cell death.

2 Mathematical Model and Experimental Method

2.1 Mathematical Model

We extend the reaction–diffusion model (1.1) to include both accidental and regulated cell death. Adopting the notation used in (1.1), we follow Tam et al. (2018) and investigate the nutrient-limited growth of a yeast colony biofilm grown on a Petri dish, and neglect the extracellular matrix as well as any mechanical effects. We assume that the mechanisms of ACD and RCD each depend exclusively on the local dimensional nutrient concentration, g^*. Deviating from Tam et al. (2018), we define the dimensional density of dead cells having undergone ACD to be $m_1^*(\boldsymbol{x}^*, t^*)$. In the model, ACD occurs when the nutrient concentration is sufficiently low. Specifically, ACD occurs when $0 < g^* < g_\dagger^*$, where $g_\dagger^*$ is a constant nutrient threshold below which ACD occurs. We assume also that the number of cells dying by ACD in unit time is proportional to the product of the dimensional living-cell density, n^* and the difference in $g_\dagger^*$ and g^*, having dimensional ACD rate constant, λ_1^*.

We assume that RCD occurs when the nutrient concentration g^* satisfies $g_1^* < g^* < g_2^*$. The constants g_1^* and g_2^* define the window within which RCD can occur. Similar to ACD, we define the dimensional RCD cell density to be $m_2^*(\boldsymbol{x}^*, t^*)$ and assume also that the number of cells dying by RCD is proportional to $n^*(g^* - g_1^*)(g_2^* - g^*)$, where λ_2^* is defined to be the dimensional RCD rate constant. As time evolves, we assume that ACD and RCD cells breakdown with respective rates γ_1^* and γ_2^*. A proportion of these broken down cells release nutrients for further consumption. We define $k_1^* \gamma_1^*$ and $k_2^* \gamma_2^*$ to be the amount of nutrient released from dead cells, per unit area, in unit time.

Given these assumptions, the coupled four-species reaction–diffusion model is:

$$
\begin{aligned}
\frac{\partial n^*}{\partial t^*} = {}& D_n^* \nabla \cdot (n^* \nabla n^*) + \alpha^* n^* g^* - \lambda_1^* n^* (g_\dagger^* - g^*) H(g_\dagger^* - g^*) \\
& - \lambda_2^* n^* (g^* - g_1^*)(g_2^* - g^*) \left[H(g^* - g_1^*) - H(g^* - g_2^*) \right],
\end{aligned}
\tag{2.1a}
$$

$$
\frac{\partial m_1^*}{\partial t^*} = D_{m1}^* \nabla^2 m_1^* + \lambda_1^* n^* (g_\dagger^* - g^*) H(g_\dagger^* - g^*) - \gamma_1^* m_1^*,
\tag{2.1b}
$$

$$
\frac{\partial m_2^*}{\partial t^*} = D_{m2}^* \nabla^2 m_2^* + \lambda_2^* n^* (g^* - g_1^*)(g_2^* - g^*) \left[H(g^* - g_1^*) - H(g^* - g_2^*) \right] - \gamma_2^* m_2^*,
\tag{2.1c}
$$

$$
\frac{\partial g^*}{\partial t^*} = D_g^* \nabla^2 g^* - c^* \alpha^* n^* g^* + k_1^* \gamma_1^* m_1^* + k_2^* \gamma_2^* m_2^*,
\tag{2.1d}
$$

where $H(\cdot)$ is the Heaviside step function. The constants D_{m1}^* and D_{m2}^* are the respective dimensional diffusivities of ACD and RCD cells.

To close the model (2.1), we require appropriate initial and boundary conditions. Since the dynamics occur within a solid Petri dish, we impose the following no-flux conditions at the boundary ∂S^*:

$$
\hat{\boldsymbol{n}} \cdot \nabla n^* = \hat{\boldsymbol{n}} \cdot \nabla m_1^* = \hat{\boldsymbol{n}} \cdot \nabla m_2^* = \hat{\boldsymbol{n}} \cdot \nabla g^* = 0 \quad \text{on} \quad \partial S^*,
\tag{2.2}
$$

where $\hat{\boldsymbol{n}}$ is the outward pointing unit normal to ∂S^*. We assume that initially there are no dead cells present, and that the nutrient concentration is spatially uniform. The initial conditions are then:

$$
n^*(\boldsymbol{x}^*, 0) = N_0^* f(\boldsymbol{x}^*),
\tag{2.3a}
$$

$$
m_1^*(\boldsymbol{x}^*, 0) \equiv 0,
\tag{2.3b}
$$

$$
m_2^*(\boldsymbol{x}^*, 0) \equiv 0,
\tag{2.3c}
$$

$$
g^*(\boldsymbol{x}^*, 0) \equiv G_0^*,
\tag{2.3d}
$$

where f is a dimensionless function controlling the initial profile of the living cells, and N_0^* and G_0^* are the initial living-cell density and nutrient concentration respectively. The governing equations (2.1) and conditions (2.2) and (2.3) define a system of four coupled partial differential equations in terms of four unknown quantities: n^*, m_1^*, m_2^*, g^*.

2.1.1 Nondimensionalisation

We nondimensionalise the system (2.1)-(2.3) by introducing the scalings:

$$n^* = N_0^* n, \qquad m_1^* = N_0^* m_1, \qquad m_2^* = N_0^* m_2,$$

$$g^* = G_0^* g, \qquad (x^*, y^*) = \sqrt{\frac{D_g^*}{\alpha^* G_0^*}}(x, y), \quad t^* = \frac{1}{\alpha^* G_0^*} t. \tag{2.4}$$

Here cell densities and the nutrient concentration have been scaled by the initial cell density and nutrient concentration, N_0^* and G_0^*, respectively. Spatial co-ordinates have been scaled with respect to the ratio between nutrient diffusion and the rate of nutrient uptake, and time has been scaled with respect to the reciprocal of the nutrient uptake rate. Substituting the scalings (2.4) into (2.1), we obtain the dimensionless system:

$$\frac{\partial n}{\partial t} = D_n \nabla \cdot (n\nabla n) + ng - \Lambda_1 n(g^\dagger - g)H(g^\dagger - g)$$
$$- \Lambda_2 n(g - g_1)(g_2 - g)\left[H(g - g_1) - H(g - g_2)\right], \tag{2.5a}$$

$$\frac{\partial m_1}{\partial t} = D_{m1}\nabla^2 m_1 + \Lambda_1 n(g^\dagger - g)H(g^\dagger - g) - \Gamma_1 m_1, \tag{2.5b}$$

$$\frac{\partial m_2}{\partial t} = D_{m2}\nabla^2 m_2 + \Lambda_2 n(g - g_1)(g_2 - g)\left[H(g - g_1) - H(g - g_2)\right] - \Gamma_2 m_2, \tag{2.5c}$$

$$\frac{\partial g}{\partial t} = \nabla^2 g - Cng + K_1 \Gamma_1 m_1 + K_2 \Gamma_2 m_2. \tag{2.5d}$$

The dimensionless system (2.5) involves the thirteen dimensionless groups:

$$D_n = \frac{N_0^* D_n^*}{D_g^*}, \quad D_{mi} = \frac{D_{mi}^*}{D_g^*}, \quad \Lambda_1 = \frac{\lambda_1^*}{\alpha^*}, \quad \Lambda_2 = \frac{\lambda_2^* G_0^*}{\alpha^*}, \quad g^\dagger = \frac{g_\dagger^*}{G_0^*},$$

$$g_i = \frac{g_i^*}{G_0^*}, \quad \Gamma_i = \frac{\gamma_i^*}{\alpha^* G_0^*}, \quad C = \frac{c^* N_0^*}{G_0^*}, \quad K_i = \frac{k_i^* N_0^*}{G_0^*}, \tag{2.6}$$

where $i \in (1, 2)$ and ∇ is now taken as the dimensionless spatially two-dimensional gradient operator. The constants D_n and D_{mi} are the ratios of the living, ACD and RCD cell diffusivity to nutrient diffusivity respectively. The groups Λ_1 and Λ_2 are respective dimensionless ACD and RCD rates. The parameters $g^\dagger$ and g_i are dimensionless nutrient thresholds. The breakdown/decay rates Γ_i represent the respective ratios of ACD and RCD breakdown rates to the nutrient uptake rate. The constant C is the rate at which nutrients deplete due to consumption by the cells, and the K_i are dimensionless measures of the quantity of nutrient released when an ACD or RCD cell breaks down. We note that the dimensional parameter k_i^* is the mass of nutrient supplied per unit cell that dies, and hence should be less than the mass of a typical eukaryotic cell (around $O(10^{-10})$). The values for N_0^*, G_0^* are estimated (see Tam et al. (2018)) to be

approximately $O(10^6)$ and $O(10^{-5})$, respectively. This gives an upper bound for K_i as $K_i < O(10)$.

From (2.2) and (2.3), the dimensionless boundary and initial conditions to be applied to (2.5) are:

$$\hat{\boldsymbol{n}} \cdot \nabla n = \hat{\boldsymbol{n}} \cdot \nabla m_1 = \hat{\boldsymbol{n}} \cdot \nabla m_2 = \hat{\boldsymbol{n}} \cdot \nabla g = 0 \quad \text{on} \quad \partial S, \quad (2.7\text{a})$$

$$n(\boldsymbol{x}, t) = f(\boldsymbol{x}) \quad \text{at} \quad t = 0, \quad (2.7\text{b})$$
$$m_1(\boldsymbol{x}, t) \equiv 0 \quad \text{at} \quad t = 0, \quad (2.7\text{c})$$
$$m_2(\boldsymbol{x}, t) \equiv 0 \quad \text{at} \quad t = 0, \quad (2.7\text{d})$$
$$g(\boldsymbol{x}, t) \equiv 1 \quad \text{at} \quad t = 0. \quad (2.7\text{e})$$

Equations (2.5) and (2.7) then form the closed dimensionless model that we investigate numerically.

2.1.2 Numerical Methods

We obtain numerical solutions to the dimensionless system (2.5) and (2.7) in one and two spatial dimensions using the method of lines. Spatial derivatives are discretised by assembling a differentiation matrix (see, *e.g.*, Driscoll and Braun (2017)) such that the interior points are discretised using a centred difference, and the boundaries are discretised using second-order accurate one-sided differences. Temporal derivatives are discretised using the first-order Euler method. In all spatially one-dimensional simulations, we chose the initial profile of the dimensionless living-cell density to be $f(x) = \exp(-x^2)$. Since this choice for f is even, and the system (2.5) contains only even derivatives in x, y, and the no-flux conditions (2.7a) are all homogeneous, it follows that solutions for n, m_1, m_2 and g are symmetric about $x = 0$ in this spatially one-dimensional case. In all spatially two-dimensional solutions, we used initial conditions that also exhibit this symmetry. Hence, in both the spatially one and two-dimensional cases, it is convenient to solve the problem numerically on $x > 0$, imposing symmetry conditions whereby the first derivative of each of the dependent variables vanishes at $x = 0$ and $y = 0$. Using this numerical method, we sought numerical solutions on a timescale longer than the actual experiment, to eliminate transient effects in which the solution behaviour is influenced by the initial condition.

2.2 Experimental Method

In this section we describe the experimental method used to obtain the results presented in Figure 1. In our experiments, three different yeast were used: *Saccharomyces cerevisiae* strains Σ1278b, (diploid, prototrophic) and W303a (*MAT*a *leu2-3,112 trp1-1 can1-100 ura3-1 ade2-1 his3-11,15 ssd1-d*), and an in-house isolate of *Magnusiomyces magnusii*. Yeast Peptone Dextrose (YPD) medium (10 g L^{-1} yeast extract, 20 g L^{-1} peptone, 20 g L^{-1} glucose) with 0.6% agar was prepared by filter sterilising 2 x YPD and mixing with an equal volume of molten 12 g L^{-1} agar. Phloxine B was

added at 10 μM. 5 mL yeast cultures were grown for 48 hours in liquid YPD prior to inoculation to plates, which was either as a 5 μM spot in the centre of medium in a 90 mm round Petri dish or as a streak, applied with a 1 μM plastic inoculation loop to medium in a 100 mm square Petri dish. Plates were cling wrapped and incubated agar side down for 10 days at 25°C. Macroscopic plate images were captured with an Apple iPhone 12 Pro and microscopic imaging. For experiments with W303a, cells were grown overnight at 30°C in YPD and colonies were grown from single cells for a period of 5 days on YPD agar plates containing 10 μM Phloxine B before images were taken using a Leica MZFLIII dissecting microscope at 10× magnification under GFP illumination (Ex488/Em520) and captured with a Cairn Scientific CellCam 200CR using ImageJ software.

3 Numerical Results and Discussion

We solve the system of equations (2.5) and (2.7) numerically in one and two spatial dimensions to investigate how ACD, RCD, cell breakdown and nutrient release influence colony biofilm growth dynamics. We show that our mathematical model is capable of reproducing qualitatively the three experimental patterns of death and morphology observed in Figure 1. The model builds on our experimental results, hypothesising that death in the colony centre is a consequence of ACD, and death near the proliferating front is a consequence of RCD.

3.1 Spatially One-Dimensional Numerical Results

Here we present spatially one-dimensional numerical solutions of (2.5) and (2.7). Our results suggest that the biofilm will grow into a state in which ACD cells are found primarily in the core of the colony (*i.e.* a necrotic core) and that RCD cells can appear in an annulus following the colony front, which then forms a plausible explanation of the patterning observed in Figure 1.

3.1.1 Colonies With ACD and No Nutrient Release Can Form a Necrotic Core

We begin by considering the case by which ACD is the only present cell-death mechanism, and examine the effect that increasing the rate of ACD has on the expansion of the colony front in the absence of breakdown ($\Gamma_1 = 0$). In the absence of cell death ($\Lambda_1 = 0$), our numerical method reproduces numerically (see Figure 2) the travelling-wave solutions obtained by Tam et al. (2018). Introducing ACD by setting $\Lambda_1 > 0$ changes the colony composition significantly. Rather than occupying the entire colony, living cells now only appear in a pulse close to the leading edge. Behind the front, the living-cell density decays, and the density of the ACD cells increases, as Figure 2 shows. This scenario represents a front of proliferating cells surrounding a large necrotic core, as observed in Figure 1A. As expected, increasing the ACD rate Λ_1 decreases the expansion speed of the colony. This effect occurs because nutrient consumption and cell proliferation drive yeast-colony expansion. Reinforcing this,
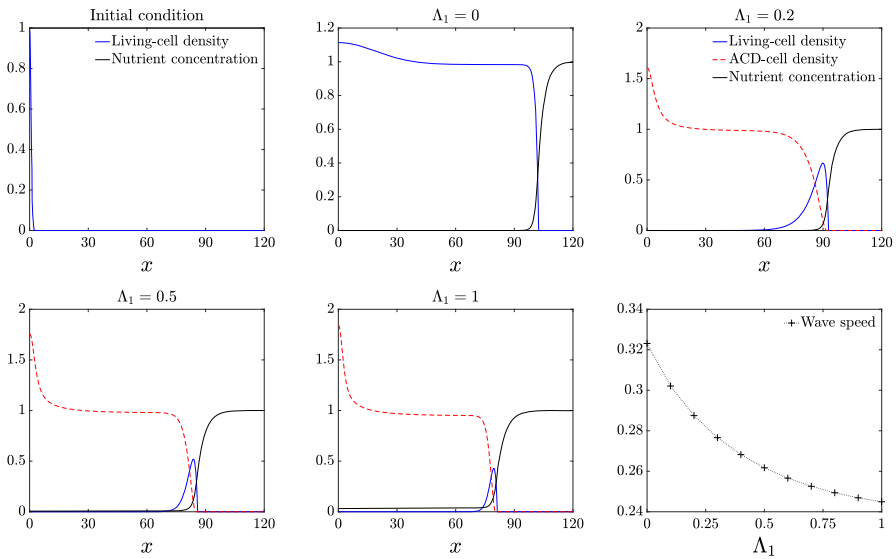
Fig. 2 Numerical solutions for the living-cell density n, ACD-cell density, m_1, and nutrient concentration g, plotted against x for increasing Λ_1. The top-left panel indicates the initial condition. The bottom-right panel shows the expansion speed plotted against Λ_1. The remaining panels indicate solutions at $t = 300$. The parameter values used used to obtain these numerical results are given by: $D_n = 0.47$, $D_{m1} = 0.001$, $C = 1$, $\Gamma_1 = 0$, $g_\dagger = 0.25$

the amplitude of the living-cell pulse monotonically decreases as the ACD rate Λ_1 is increased. Without subsequent ACD breakdown and nutrient release, the ACD-cell density settles to the constant value $1/C$. For small Λ_1, living cells are capable of consuming all of the nutrient at the centre of the colony. If the rate of ACD is sufficiently large, for example $\Lambda_1 = 1$, we find that the cells die before all of the nutrient is consumed.

We now consider the effect of cell breakdown and nutrient release for the case in which ACD is the only present cell-death mechanism. As we see in Figure 3, for sufficiently small values of the ACD nutrient-release parameter K_1, the pulse profile for the living cells that occurs with no nutrient release is preserved. As K_1 increases, the pulse increases in amplitude and width. Expansion speed also increases approximately linearly with the amount of nutrients released K_1. Increasing K_1 provides the colony with more nutrient, facilitating more cell proliferation, increased cell density, and faster expansion. Unlike in Figure 2, the ACD-cell density takes a pulse profile, due to the breakdown of cells behind the front. For sufficiently large K_1, enough nutrient is released to the colony that the living-cell density transitions to a wave-front profile, such that living cells, ACD cells, and nutrient are all present throughout the colony.
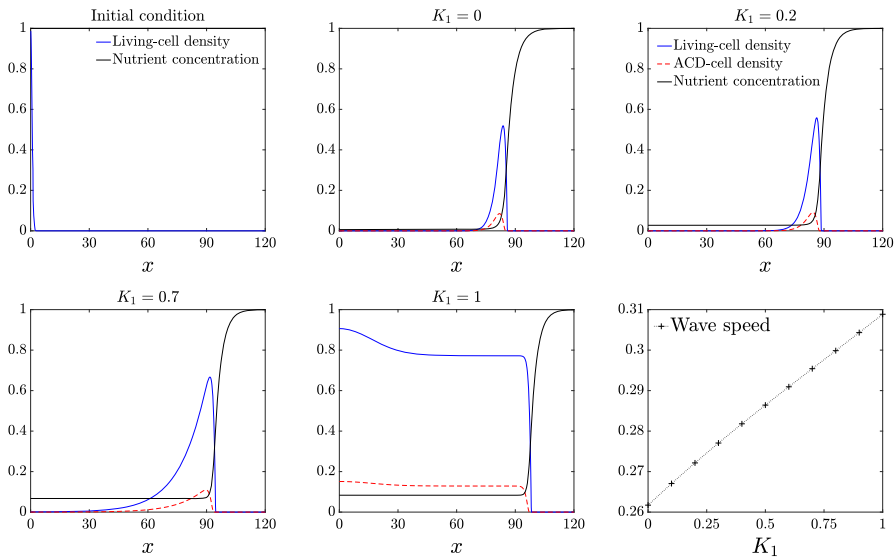
Fig. 3 Numerical solutions for the living-cell density n, ACD-cell density, m_1, and nutrient concentration g, plotted as a function of x for increasing K_1. The top-left panel indicates the initial condition. The bottom-right panel shows the expansion speed plotted against K_1. The remaining panels indicate solutions at $t = 300$. The parameter values used for this simulation are: $\Lambda_1 = 0.5$, $D_n = 0.47$, $D_{m1} = 0.001$, $C = 1$, $\Gamma_1 = 0.5$, $g_\dagger = 0.25$

3.1.2 Colonies with ACD, RCD, and nutrient release can have death in an edge-trailing ring and in the core

We now investigate the phenotype in Figure 1B, where there is a core of dead cells, and a distinct ring of dead cells trailing the front. We show that introducing RCD at a higher rate than ACD can give rise to this ring structure. We consider the case in which the rate of ACD breakdown and nutrient release is much smaller than the corresponding RCD rate. As the rate of RCD breakdown increases, the rate at which nutrient is released back to the colony is increased, increasing its expansion speed. Examining Figure 4, in contrast to Figure 2 and 3, a dominant RCD rate means that the living cells occupy the entire domain. Since ACD is low, living cells can persist in the core where nutrient concentration is low. Although the number of ACD cells is small overall, they are maximised in the colony centre ($x = 0$), and decrease approximately linearly away from the centre. On the other hand, RCD occurs with maximum rate at an intermediate nutrient concentration. When RCD cells break down, the distribution of RCD cells takes the form of a pulse following the leading edge, whose amplitude is modulated by the RCD breakdown rate, Γ_2. Under the assumption of radial symmetry, this would appear as a red ring following closely behind the front, and so could be representative of the experimental result presented in Figure 1B. In this experiment, there is a less-pronounced region of dead cells in the centre of the colony, which these solutions predict to be ACD cells. If the RCD breakdown rate Γ_2 is small, the ratio of RCD to ACD cells increases, because small Γ_2 increases the amplitude of the RCD pulse. As
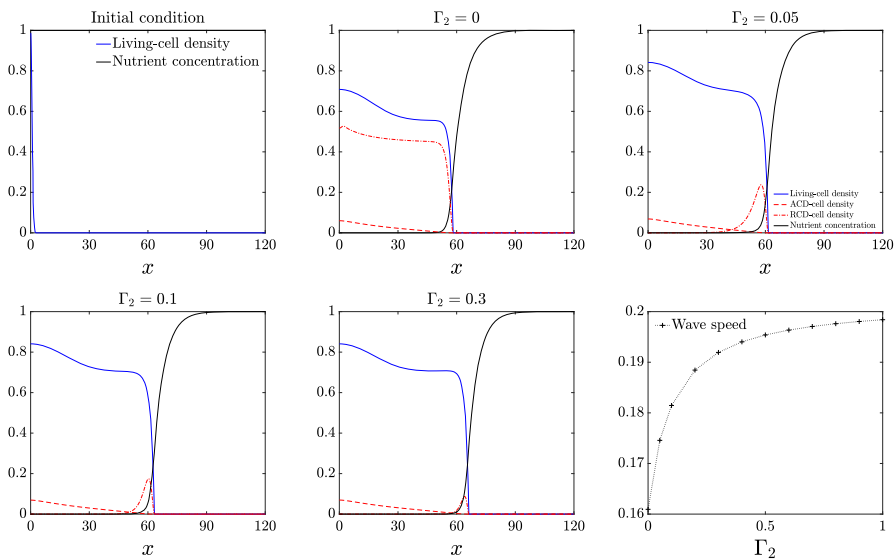
Fig. 4 Numerical solutions for the living-cell density n, ACD-cell density, m_1, RCD-cell density, m_2, and nutrient concentration, g, plotted at $t = 300$ against x with $K_1 = 0$, $K_2 = 0.5$ and increasing Γ_2. The top-left panel indicates the initial condition. The bottom-right panel shows the expansion speed plotted against Γ_2. The remaining parameter values used for this simulation are: $D_n = 0.47$, $D_{m1} = 0.001$, $\Lambda_1 = 0.001$, $\Lambda_2 = 0.5$, $C = 1$, $\Gamma_1 = 0$, $g_\dagger = 0.25$, $g_1 = 0$, $g_2 = 1$

the colony expands, the nutrient concentration decays, meaning that the rate of RCD is reduced. Since the rate of RCD is significantly larger than ACD, the colony is able to maintain life in the core. Interestingly, the bottom-right panel of Figure 4 demonstrates that even small RCD breakdown rates yield comparatively large increases in expansion speed. We hypothesise that the ring phenotype in Figure 1B might occur due to fast RCD compared to ACD and a sufficiently low rate of nutrient release. Even a small amount of nutrient release would be sufficient to increase colony expansion speed, and would correspond to the most pronounced cell-death ring pattern trailing the leading edge.

Whilst the most meaningful parameter set is the one for which the nutrient release rate of the RCD cells dominate those of ACD (Figure 4), we also chose to run a simulation such that ACD and RCD are both present, where both species are capable of releasing nutrient at similar rates and quantities. The results in this case show that the (relatively fast) breakdown of the ACD cells produces a similar pulse profile for the ACD cells as was for the RCD cells in Figure 4.

3.2 Spatially Two-Dimensional Numerical Results

The spatially one-dimensional solutions in Section 3.1 apply to the experiments of Figure 1A–B, where the patterns exhibit approximate radial symmetry. In the absence of cell death ($m_1 \equiv m_2 \equiv 0$), it has previously been shown that planar travelling-wave solutions to the model (2.5) can be linearly unstable to transverse sinusoidal perturba-
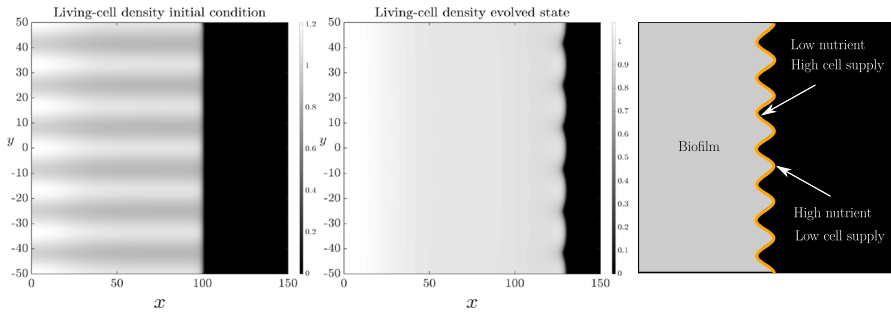
Fig. 5 Spatially two-dimensional numerical solution of (2.5) and (2.7a) subject to the transversely perturbed initial condition (3.1) on the domain $x \in (0, 150)$, $y \in (-50, 50)$ in the absence of cell death. The first panel shows the initial condition, the centre panel shows the corresponding solution at $t = 100$, and the final panel is a schematic illustrating the instability mechanism. The specific parameter values that have been used are: $D_n = 0.47$, $C = 1$, $\Lambda_1 = 0$, $\Lambda_2 = 0$, $\delta = 0.1$, $q = 6\pi/50$

tions (Müller and van Saarloos 2002; Tam et al. 2018). We now investigate numerically the spatiotemporal stability of the spatially one-dimensional solutions obtained in Section 3.1 to qualitatively understand how cell death affects colony morphology. We use the spatially one-dimensional numerical solutions to (2.5) and (2.7) at $t = 300$ as the base states for our numerical linear stability analysis, and denote these solutions respectively as: n_0, m_{10}, m_{20}, and g_0. We then use transversely perturbed versions of these solutions as initial conditions to obtain spatially two-dimensional numerical solutions of (2.5) and (2.7), and observe how the perturbations evolve over time. Formally, the initial conditions used for the two-dimensional simulations are:

$$n(x, y) = n_0(x)\left(1 + \delta \cos(qy)\right), \tag{3.1a}$$

$$m_1(x, y) = m_{10}(x)\left(1 + \delta \cos(qy)\right), \tag{3.1b}$$

$$m_2(x, y) = m_{20}(x)\left(1 + \delta \cos(qy)\right), \tag{3.1c}$$

$$g(x, y) = g_0(x)\left(1 + \delta \cos(qy)\right), \tag{3.1d}$$

where $0 < \delta \ll 1$ is the initial amplitude of the perturbation, and $q > 0$ is the wavenumber. Planar front solutions to (2.5) without cell death can be unstable to long-wavelength (small q) transverse perturbations, depending on the ratio of cell diffusivity to nutrient diffusivity (Müller and van Saarloos 2002; Tam et al. 2018). In all solutions, we use $\delta = 0.1$ and $q = 6\pi/50 = 0.3770$, which is close to the most unstable wave number for $D = 0.47$, determined by Müller and van Saarloos (2002) and it is noted that the timescale on which the spatially two-dimensional results are valid is one for which the amplitude of the perturbation remains small. In Figure 5A, we reproduce numerically the unstable floral morphology with these parameters in the absence of cell death.

Figure 5B illustrates the mechanism of the instability. As Müller and van Saarloos (2002) explain, when the front is perturbed there is a trade-off between nutrient supply, which amplifies the perturbation, and cell diffusivity, which smooths the perturbation. When the colony protrudes ahead of the undisturbed front, it enters a comparatively
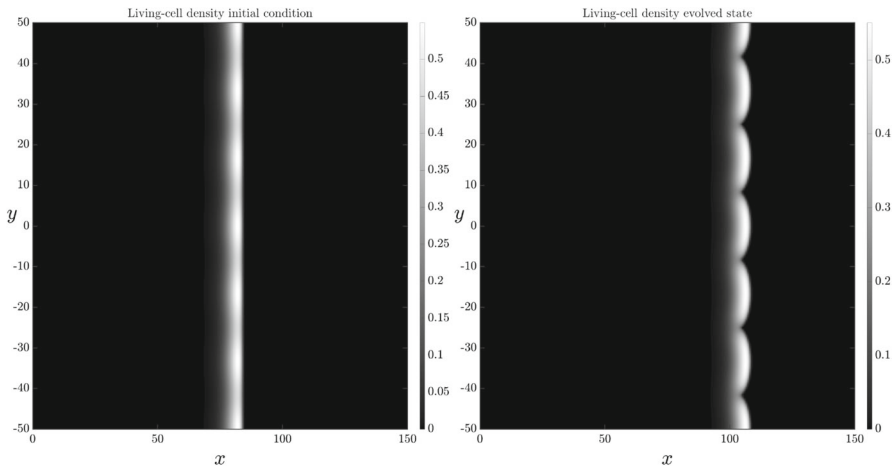
Fig. 6 Spatially two-dimensional numerical solution of (2.5) and (2.7a) subject to the transversely perturbed initial condition (3.1) on the domain $x \in (0, 150)$, $y \in (-50, 50)$. There is ACD, but no nutrient release or RCD. The left-hand panel shows the initial condition. The right-hand panel shows the solution at $t = 100$. The parameter values that have been used are: $D_n = 0.47$, $C = 1$, $\Lambda_1 = 0.5$, $\Lambda_2 = 0$, $\Gamma_1 = 0$, $K_1 = 0$

nutrient-rich region, which aids cell proliferation and further protrusion. Nutrients are more depleted behind the undisturbed front, inhibiting cell proliferation there. Cell diffusion counteracts the destabilising effect of nutrient supply by supplying cells to the interface from behind. This cell supply occurs more readily to non-protruded regions than to protrusions, stabilising the interface (Müller and van Saarloos 2002). Due to these competing effects, increasing the ratio of cellular diffusivity to nutrient diffusivity suppresses the instability for larger wavenumber, shorter-wavelength modes (Müller and van Saarloos 2002). For sufficiently large D_n, the instability is completely eliminated for all modes (Müller and van Saarloos 2002). Using spatially two-dimensional numerical solutions, we will investigate qualitatively how cell death influences these instability dynamics. Since the growth rates of these transverse perturbations are small (Müller and van Saarloos 2002), we explore the instability numerically, solving until $t = 100$, which is beyond the experimental regime.

3.2.1 Cell Death Amplifies Floral Pattern Formation

Cell death affects the balance between cell diffusion and nutrient supply, and hence the instability mechanism described in Section 3.2. Spatially two-dimensional numerical solutions with cell death present support this idea. Figure 6 shows spatially two-dimensional solutions of (2.5), (2.7a) and (3.1), for the case in which ACD is the only present cell-death mechanism, and in the absence of cellular breakdown and nutrient release. The results indicate the stability of the spatially one-dimensional numerical results presented in Figure 2.

Qualitatively, it is observed that ACD in isolation amplifies the instability, having increased petal protrusion compared to Figure 5, where there was zero cell death. With ACD present, but in the absence of nutrient release, the amplitude of the living-cell
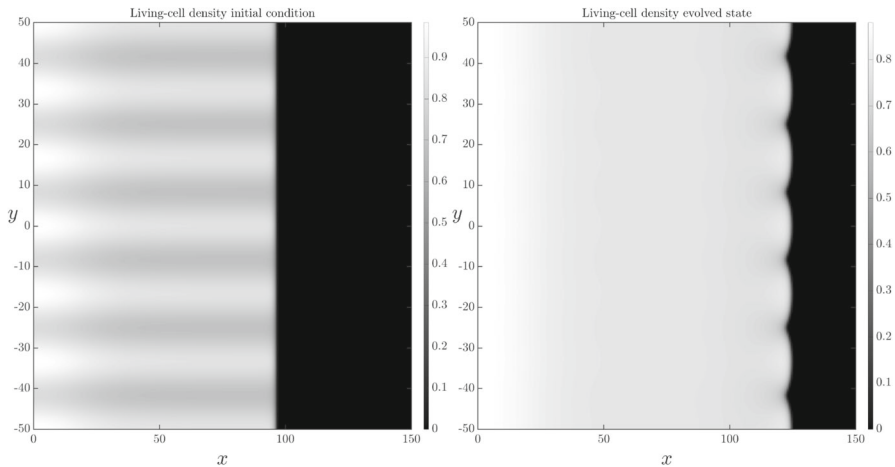
Fig. 7 Spatially two-dimensional numerical solution of (2.5) and (2.7a) subject to the transversely perturbed initial condition (3.1) on the domain $x \in (0, 150)$, $y \in (-50, 50)$. There is ACD and nutrient release, but no RCD. The left-hand panel shows the initial condition. The right-hand panel shows the solution at time $t = 100$. The parameter values that have been used are: $D_n = 0.47$, $C = 1$, $\Lambda_1 = 0.5$, $\Lambda_2 = 0$, $\Gamma_1 = 0.5$, $K_1 = 1$

density declines with increasing Λ_1, as Figure 2 shows. This decrease in cell density decreases cell supply to the interface from behind, suppressing the stabilising impact of cell diffusion. Since there is no nutrient release, the destabilising effect of the nutrient concentration is unchanged. The net result is an increase in petal amplitude.

With nutrient release from ACD-cell breakdown, nutrient is resupplied to the colony behind the leading edge. This lessens the difference in nutrient concentration ahead and behind the colony front, reducing the instability. It also facilitates more cell proliferation, and hence increases the living-cell density compared to the scenario with no nutrient release. This higher cell density neutralises the suppression of cell supply to the interface discussed above. Therefore, nutrient release tends to lessen the floral instability. This effect occurs in Figure 7, where petal amplitude is similar to, but smaller than, the petal size with ACD only and no nutrient release (Figure 6).

In Section 3.1 it was shown that a combination of ACD and RCD capable of breakdown and nutrient release can produce the spatial patterns observed in Figure 1B. We now explore numerically how these features influence the instability by perturbing the solutions presented in Figure 4. With the low rate of nutrient release that yielded the ring, Figure 8 shows that the interface remains unstable. However, the combination of ACD and RCD decreases the petal amplitude. This reduction in amplitude is due to the fact that RCD and nutrient recovery occurs near the proliferating rim, promoting cell proliferation there. Cell proliferation increases the living-cell density, inhibiting the floral instability. Our results suggest that the primary function of RCD and nutrient release is to increase the overall colony expansion speed, and not necessarily enhance petal formation. In less favourable conditions, the floral morphology might help the yeast colony to more easily invade previously unoccupied regions, and increase overall nutrient supply to the cells. Nutrient release from dead cells improves the growth
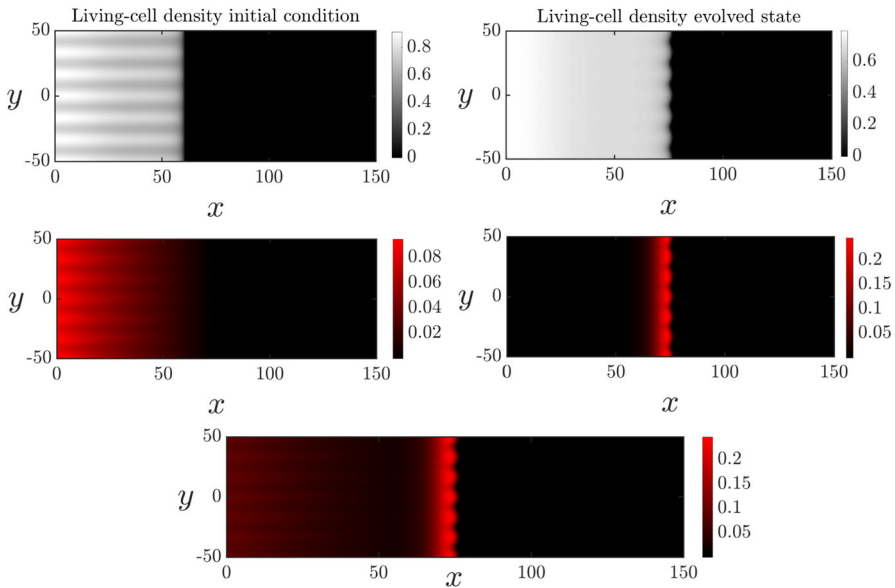
Fig. 8 Spatially two-dimensional numerical solution of (2.5) and (2.7a) subject to the transversely perturbed initial condition (3.1) on the domain $x \in (0, 150)$, $y \in (-50, 50)$. There is ACD, RCD and nutrient release. The top row shows the living-cell density in its initial (left) and evolved (state). The middle panel shows the ACD-cell density (left) and RCD-cell density (right) in their evolved states. The bottom panel shows the sum $m_1 + m_2$ of the dead cell densities. The parameter values that were used are: $D_n = 0.47$, $C = 1$, $\Lambda_1 = 0.001$, $\Lambda_2 = 0.5$, $\Gamma_1 = 0$, $\Gamma_2 = 0.05$, $K_2 = 0.5$

conditions near the leading edge. Therefore, there is less need for amplified petal formation as the colony expands, even though the instability persists.

3.2.2 Solutions With Linear Cell Diffusion Do Not Develop Floral Morphology

Previous works have shown that nonlinear cell diffusion is required for planar-front solutions of our model (2.5) in the absence of cell death to be unstable (Müller and van Saarloos 2002), and that planar fronts are stable with linear cell diffusion (Ben-Jacob et al. 2000). Here we demonstrate that this is also the case when cell death is present. To do this, we modified the system (2.5) by exchanging nonlinear diffusion in the living-cell density for linear (Fickian) cell diffusion. This modified system was then solved with the effects of ACD, RCD, and nutrient release all present. The corresponding numerical results are shown in Figure 9, where it is observed that linear diffusion results in an apparently stable planar front. Therefore, although cell death can amplify the petal-forming instability, nonlinear cell diffusivity is the instability mechanism.

Since yeast cells are immotile, living-cell diffusion is a phenomenological description for how cells colonise the Petri dish. Nonlinear cell diffusivity has been justified because it yields solutions with compactly-supported cell density, as occurs in experiments. Nonlinear diffusivity might also arise due to random movement of cells with aspect ratios not equal to unity (Simpson et al. 2011), and also because the diffusive flux (spread of cells) increases with elevated cell density, in addition to the cell-density
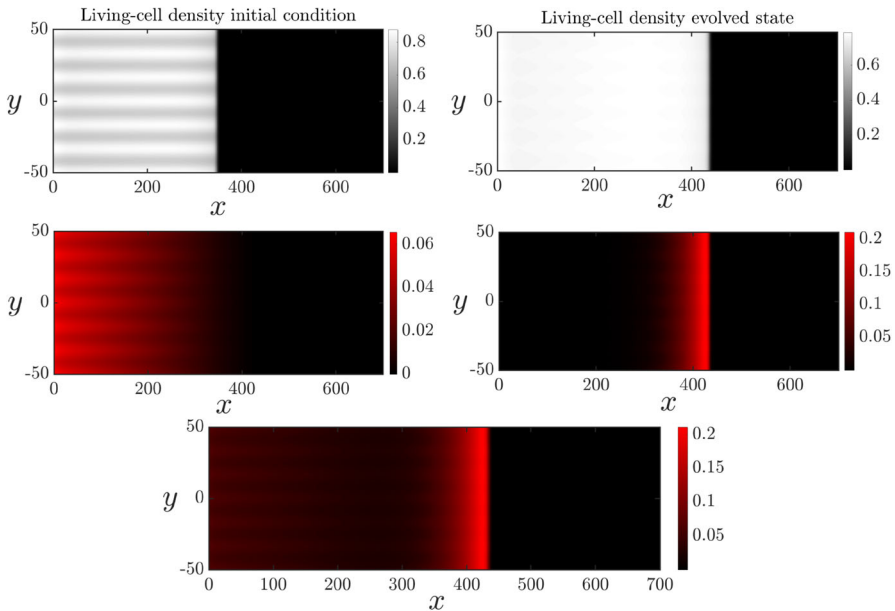
Fig. 9 Spatially two-dimensional numerical solution of (2.5) and (2.7a) subject to the transversely perturbed initial condition (3.1) on the domain $x \in (0, 700)$, $y \in (-50, 50)$ for the case of linear diffusion. The parameters were chosen to match Figure 8

gradient. However, since cell diffusivity is phenomenological, the most suitable cellular diffusivity that corresponds to experiments is unknown. In Figure 1, the colonies in Panels A and B have little floral pattern formation, whereas the colony in Panel C does have a floral pattern. Since nonlinear cell diffusivity predicts slow-growing instability, we cannot determine whether the experiments in Panels A and B are too early to observe the instability, or whether the instability will never develop. Both Figure 8 and 9 indicate the ring of cell death. Therefore, the broad impact of ACD and RCD on the distribution of living and dead cells is independent of the choice of cellular diffusivity.

4 Conclusions

Yeasts can alter their growth to adapt to different environments. These adaptations help yeasts to survive in both natural environments and controlled laboratory experiments. In this article, we have used experiments and mathematical modelling to investigate the effects of accidental cell death (ACD) and regulated cell death (RCD) on the nutrient-limited growth of yeast colony biofilms.

We used the vitality dye Phloxine B to indicate regions of elevated cell death in yeast colony biofilms. Our experiments reveal three patterns of cell death. One pattern involves a colony that develops a region of cell death at the centre, with living cells being found closer to the proliferating rim. In a different experiment, the most

pronounced region of cell death occured in a ring that trails the leading edge. This experiment was also replicated in a rectangular Petri dish, where we observed a region of cell death trailing the front, which evolves into a non-uniform spatial pattern. Our objective was to develop a mathematical model that could explain the three patterns of cell death observed in experiments.

Distinguishing between ACD and RCD helps to formulate a potential explanation for the different colony patterns observed in Figure 1. ACD occurs in harsh environments, where the cell is unable to sustain life. RCD occurs when a cell would be able to survive, but instead elects to die in response to an environmental cue. RCD is altruistic, where the death benefits the colony as a whole. The benefit to the colony is hypothesised here as being due to the release of nutrients back to the colony. Nearby cells can then consume the returned nutrients, spurring increased cell proliferation and colony expansion.

In this work, we have extended an existing reaction–diffusion model for the expansion of yeast colony biofilms (Müller and van Saarloos 2002; Tam et al. 2018) to incorporate the effects of ACD and RCD. This extended system involves four coupled nonlinear partial differential equations, which collectively describe the spatiotemporal evolution of the living cells and nutrient concentration within the colony, as well as two species of dead cells: those that have died by either ACD or RCD. Numerical solutions of this extended system were shown to reproduce qualitatively the patterning observed in our experiments. In the absence of RCD, we used our model to demonstrate that the colony can form a necrotic-core-like composition, with living cells mostly being found close to the leading edge. If RCD is introduced, the colony takes a more complex composition. In this case, living cells will, in general, persist throughout the colony. Cells that die by ACD are most abundant in the centre, and cells dying by RCD occur in a pulse close to the leading edge. This behaviour is reminiscent of the experimental ring phenotype in Figure 1B. Varying model parameters demonstrated that the breakdown of RCD cells together with nutrient release can increase the speed of expansion. The impact on expansion speed is greatest at low amounts of RCD breakdown, whereas large amounts of breakdown incur diminishing returns. Our model suggests that even small amounts of RCD can be impactful for colony expansion.

Numerical solutions in two spatial dimensions enabled us to investigate the non-uniform front patterns observed in our rectangular experiments Figure 1C. Previous work by Müller and van Saarloos (2002) shows that a reaction–diffusion model without cell death could predict petal-like structure formation in yeast colony biofilms (Tam et al. 2018). These petals are advantageous for colony growth, enabling regions of the colony boundary to invade unoccupied regions faster. Our results demonstrate that, although cell death slows overall expansion (relative to the death-free case), it enhances petal formation. This enhanced petal formation could be a secondary advantage to the colony. Like previous mathematical models (Müller and van Saarloos 2002; Hilhorst et al. 2008), nonlinear cell diffusion was necessary for our model to give rise to spatially unstable numerical solutions.

Careful interpretation of our results requires considering some limitations to this study. Introducing ACD and RCD to existing models for nutrient-limited colony biofilm growth generates a system of four coupled reaction–diffusion equations. It also requires introducing new parameters, specifically, the rate of ACD and RCD,

the rate of cellular breakdown and nutrient release, the proportion of nutrient that can be re-consumed, and the nutrient concentration thresholds at which ACD and RCD occur. The results presented in this paper are only a subset of the possible behaviours, and depend on the choices of parameter values. Furthermore, previous minimal reaction–diffusion systems were amenable to travelling-wave analysis and linear stability analysis. Since each reaction–diffusion equation is second-order, performing a travelling-wave analysis of the model with cell death would involve the complicated task of analysing an eight-dimensional dynamical system. Without this analysis, we do not have theoretical predictions of the expansion speed or the growth rate of perturbations in the two-dimensional solutions, and instead rely on numerical solutions to analyse the model qualitatively. Another limitation is that the Phloxine B dye cannot distinguish between accidental and regulated cell death. Although experimentalists believe that the trailing ring of cell death is due to regulated cell death, we are unable to confirm this definitively. Consequently, the key contribution of this work is using the mathematical model to generate a theoretical hypothesis for how RCD might be responsible for the observed cell-death patterns. Future experimental work could focus on isolating the nature of cell death in either the core or the outer ring.

Author Contributions   DJN: Methodology, software, validation, formal analysis, investigation, writing — original draft, writing — review & editing, visualisation.
AKYT: Methodology, writing — original draft, writing — review & editing, supervision, funding acquisition.
JEFG: Conceptualization, methodology, writing — review & editing, supervision, funding acquisition.
TK: Investigation, data curation.
JMG: Investigation, data curation, writing — original draft, supervision.
CWG: Conceptualization, methodology, investigation, data curation, writing — original draft, writing — review & editing, writing — review & editing, funding acquisition.
VJ: Conceptualization, writing — review & editing, supervision, funding acquisition.
BJB: Conceptualization, methodology, writing — review & editing, supervision, project administration, funding acquisition.

Data Availability Numerical code is available on request.

Declarations

Competing Interests We have no competing interests to declare.

References

Andersen KS, Bojsen R, Sørensen L, Nielsen MW, Lisby M, Folkesson A, Regenberg B (2014) Genetic basis for *Saccharomyces cerevisiae* biofilm in liquid medium. G3 (Bethesda) 4(9):1671–1680. https://doi.org/10.1534/g3.114.010892

Asally M, Kittisopikul M, Rué P, Du Y, Hu Z, Çağatay T, Robinson AB, Lu H, Garcia-Ojalvo J, Süel GM (2012) Localized cell death focuses mechanical forces during 3D patterning in a biofilm. Proc Natl Acad Sci USA 109(46):18891–18896. https://doi.org/10.1073/pnas.1212429109

Beauvais A, Loussert C, Prevost MC, Verstrepen K, Latgé JP (2009) Characterization of a biofilm-like extracellular matrix in FLO1-expressing *Saccharomyces cerevisiae* cells. FEMS Yeast Res 9(3):411–419. https://doi.org/10.1111/j.1567-1364.2009.00482.x

Ben-Jacob E, Cohen I, Levine H (2000) Cooperative self-organization of microorganisms. Adv Phys 49(4):395–554. https://doi.org/10.1080/000187300405228

Bojsen RK, Andersen KS, Regenberg B (2012) Saccharomyces Cerevisiae – a model to uncover molecular mechanisms for yeast biofilm biology. FEMS Immunol Med Microbiol 65(2):169–182. https://doi.org/10.1111/j.1574-695X.2012.00943.x

Byrne HM, Chaplain M (1996) Modelling the role of cell-cell adhesion in the growth and development of carcinomas. Math Comput Model 24(12):1–17. https://doi.org/10.1016/s0895-7177(96)00174-4

Byrne HM, King JR, McElwain D, Preziosi L (2003) A two-phase model of solid tumour growth. Appl Math Lett 16(4):567–573. https://doi.org/10.1016/S0893-9659(03)00038-7

Cannon JF, Gibbs JB, Tatchell K (1986) Supperssors of the Ras2 mutation of Saccharomyces cerevisiae. Genetics 113(2):247–264. https://doi.org/10.1093/genetics/113.2.247

Čáp M, Štěpánek L, Harant K, Váchová L, Palková Z (2012) Cell differentiation within a yeast colony: Metabolic and regulatory parallels with a tumor-affected organism. Mol Cell 46(4):436–448. https://doi.org/10.1016/j.molcel.2012.04.001

Carmona-Gutierrez D, Bauer MA, Zimmermann A, Aguilera A, Austriaco N, Ayscough K, Balzan R, Bar-Nun S, Barrientos A, Belenky P, Blondel M, Braun RJ, Breitenbach M, Burhans WC, Büttner S, Cavalieri D, Chang M, Cooper KF, Côrte-Real M, Costa V, Cullin C, Dawes I, Dengjel J, Dickman MB, Eisenberg T, Fahrenkrog B, Fasel N, Fröhlich KU, Gargouri A, Giannattasio S, Goffrini P, Gourlay CW, Grant CM, Greenwood MT, Guaragnella N, Heger T, Heinisch J, Herker E, Herrmann JM, Hofer S, Jiménez-Ruiz A, Jungwirth H, Kainz K, Kontoyiannis DP, Ludovico P, Manon S, Martegani E, Mazzoni C, Megeney LA, Meisinger C, Nielsen J, Nyström T, Osiewacz HD, Outeiro TF, Park H, Pendl T, Petranovic D, Picot S, Polčic P, Powers T, Ramsdale M, Rinnerthaler M, Rockenfeller P, Ruckenstuhl C, Schaffrath R, Segovia M, Severin FF, Sharon A, Sigrist SJ, Sommer-Ruck C, Sousa MJ, Thevelein JM, Thevissen K, Titorenko V, Toledano MB, Tuite M, Vögtle FN, Westermann B, Winderickx J, Wissing S, Wölfl S, Zhang ZJ, Zhao RY, Zhou B, Galluzzi L, Kroemer G, Madeo F (2018) Guidelines and recommendations on yeast cell death nomenclature. Microb Cell 5(1):4–31. https://doi.org/10.15698/mic2018.01.607

Chen L, Noorbakhsh J, Adams RM, Samaniego-Evans J, Agollah G, Nevozhay D, Kuzdzal-Fick J, Mehta P, Balázsi G (2014) Two-dimensonality of yeast colony expansion accompanied by pattern formation. PLoS Comput Biol 10(12):1003979. https://doi.org/10.1371/journal.pcbi.1003979

Clarelli F, Di Russo C, Natalini R, Ribot M (2015) A fluid dynamics multidimensional model of biofilm growth: Stability, influence of environment and sensitivity. Math Med Biol 33(4):371–395. https://doi.org/10.1093/imammb/dqv024

Costerton JW, Stewart PS, Greenberg EP (1999) Bacterial biofilms: A common cause of persistent infections. Science 284(5418):1318–1322. https://doi.org/10.1126/science.284.5418.1318

Dockery J, Klapper I (2001) Finger formation in biofilm layers. SIAM J Appl Math 62(3):853–869. https://doi.org/10.1137/s0036139900371709

Driscoll TA, Braun RJ (2017) Fundamentals of Numerical Computation. Other Titles in Applied Mathematics. SIAM, Delaware, USA. https://doi.org/10.1137/1.9781611975086

Eberl HJ, Parker DF, van Loosdrecht M (2001) A new deterministic spatio-temporal continuum model for biofilm development. J Theor Med 3(3):161–175. https://doi.org/10.1080/10273660108833072

Flemming H, Wingender J (2010) The biofilm matrix. Nat Rev Microbiol 8(9):623–633. https://doi.org/10.1038/nrmicro2415

Gallegos A, Mazzag B, Mogilner A (2006) Two continuum models for the spreading of myxobacteria swarms. Bull Math Biol 68(4):837–861. https://doi.org/10.1007/s11538-005-9031-2

Ghosh P, Levine H (2017) Morphodynamics of a growing microbial colony driven by cell death. Phys Rev E 96(5):052404. https://doi.org/10.1103/PhysRevE.96.052404

Gimeno CJ, Ljungdahl PO, Styles CA, Fink GR (1992) Unipolar cell divisions in the yeast *S. cerevisiae* lead to filamentous growth: Regulation by starvation and RAS. Cell 68(6):1077–1090. https://doi.org/10.1016/0092-8674(92)90079-R

Giverso C, Verani M, Ciarletta P (2015) Branching instability in expanding bacterial colonies. J R Soc Interface 12(104):20141290. https://doi.org/10.1098/rsif.2014.1290

Goffeau A, Barrell BG, Bussey H, Davis RW, Dujon B, Feldmann H, Galibert F, Hoheisel JD, Jacq C, Johnston M, Louis EJ, Mewes HW, Murakami Y, Philippsen P, Tettelin H, Oliver SG (1996) Life with 6000 genes. Science 274(5287):546–567. https://doi.org/10.1126/science.274.5287.546

Gourlay CW, Du W, Ayscough KR (2006) Apoptosis in yeast - mechanisms and benefits to a unicellular organism. Mol Microbiol 62(6):1515–1521. https://doi.org/10.1111/j.1365-2958.2006.05486.x

Gray BF, Kirwan NA (1974) Growth rates of yeast colonies on solid media. Biophys Chem 1(3):204–213. https://doi.org/10.1016/0301-4622(74)80006-2

Greenspan HP (1972) Models for the growth of a solid tumor by diffusion. Stud Appl Math 51(4):317–340. https://doi.org/10.1002/sapm1972514317

Hilhorst D, Kersner R, Logak E, Mimura M (2008) Interface dynamics of the Fisher equation with degenerate diffusion. J Differ Equ 244(11):2870–2889. https://doi.org/10.1016/j.jde.2008.02.018

Horváth D, Petrov V, Scott SK, Showalter K (1993) Instabilities in propagating reaction-diffusion fronts. J Chem Phys 98(8):6332–6343. https://doi.org/10.1063/1.465062

Kawasaki K, Mochizuki A, Matsushita M, Umeda T, Shigesada N (1997) Modeling spatio-temporal patterns generated by *Bacillus subtilis*. J Theor Biol 188(2):177–185. https://doi.org/10.1006/jtbi.1997.0462

Kitsunezaki S (1997) Interface dynamics for bacterial colony formation. J Phys Soc Jpn 66:1544–1550. https://doi.org/10.1143/JPSJ.66.1544

Klapper I, Dockery J (2010) Mathematical description of microbial biofilms. SIAM Rev 52(2):221–265. https://doi.org/10.1137/080739720

Laspidou CS, Rittmann BE (2002) a unified theory for extracellular polymeric substances, soluble microbial products, and active and inert biomass. Water Res 36(11):2711–2720

Laspidou C, Rittmann B (2004) modeling biofilm complexity by including active and inert biomass and extracellular polymeric substances. Biofilms 1(4):285–291

Leadsham JE, Miller K, Ayscough KR, Colombo S, Martegani E, Sudbery P, Gourlay CW (2009) Whi2p links nutritional sensing to actin-dependent Ras-cAMP-PKA regulation and apoptosis in yeast. J Cell Sci 122(5):706–715. https://doi.org/10.1242/jcs.042424

Leadsham JE, Kotiadis VN, Tarrant DJ, Gourlay CW (2010) Apoptosis and the yeast actin cytoskeleton. Cell Death Differ 17(5):754–762. https://doi.org/10.1038/cdd.2009.196

Lega J, Passot T (2003) Hydrodynamics of bacterial colonies: A model. Phys Rev E 67(3):031906. https://doi.org/10.1103/physreve.67.031906

Li K, Green J, Tronnolone H, Tam A, Black AJ, Gardner JM, Sundstrom JF, Jiranek V, Binder BJ (2024) An off-lattice discrete model to characterise filamentous yeast colony morphology. PLoS Comput, Biol

Martinez LM, Fries BC (2010) Fungal biofilms: Relevance in the setting of human disease. Curr Fungal Infect Rep 4(4):266–275. https://doi.org/10.1007/s12281-010-0035-5

Mattei MR, Frunzo L, D'Acunto B, Pechaud Y, Pirozzi F, Esposito G (2018) Continuum and discrete approach in modeling biofilm development and structure: A review. J Math Biol 76(4):945–1003. https://doi.org/10.1007/s00285-017-1165-y

Middelhoven WJ, Broekhuizen B, van Eijk J (1976) Detection, with the dye phloxine B, of yeast mutants unable to utilize nitrogenous substances as the sole nitrogen source. J Bacteriol 128(3):851–852. https://doi.org/10.1128/jb.128.3.851-852.1976

Minois N, Frajnt M, Wilson C, Vaupel JW (2005) Advances in measuring lifespan in the yeast *Saccharomyces cerevisiae*. Proc Natl Acad Sci USA 102(2):402–406. https://doi.org/10.1073/pnas.0408332102

Müller J, van Saarloos W (2002) Morphological instability and dynamics of fronts in bacterial growth models with nonlinear diffusion. Phys Rev E 65(6):061111. https://doi.org/10.1103/PhysRevE.65.061111

Oelker AC (2017) Mathematical modeling and pattern formation for bacterial colonies. PhD thesis, Technische Universität München

Pappas PG, Lionakis MS, Arendrup MC, Ostrosky-Zeichner L, Kullberg BJ (2018) Invasive candidiasis. Nat Rev Dis Primers 4(1):18026. https://doi.org/10.1038/nrdp.2018.26

Peck VM, Fuge EK, Padilla PA, Gomez MA, Werner-Washburne M (1997) Yeast Bcy1 mutants with stationary phase-specific defects. Curr Genet 32(2):83–92. https://doi.org/10.1007/s002940050251

Pentland DR, Davis J, Mühlschlegel FA, Gourlay CW (2021) CO_2 enhances the formation, nutrient scavenging and drug resistance properties of *C. albicans* biofilms. Npj Biofilms Microbiomes 7(1):67. https://doi.org/10.1038/s41522-021-00238-z

Picioreanu C, van Loosdrecht MCM, Heijnen JJ (1998) Mathematical modeling of biofilm structure with a hybrid differential-discrete cellular automaton approach. Biotechnol Bioeng 58(1):101–116. 10.1002/670(SICI)1097-0290(19980405)58:1<101::AID-BIT11>3.0.CO;2-M

Plocek V, Váchová L, Šťovíček V, Palková Z (2020) Cell distribution within yeast colonies and colony biofilms: How structure develops. Int J Mol Sci 21:3873. https://doi.org/10.3390/ijms21113873

Reynolds TB, Fink GR (2001) Bakers' yeast, a model for fungal biofilm formation. Science 291(5505):878–881. https://doi.org/10.1126/science.291.5505.878

Reynolds TB, Jansen A, Peng X, Fink GR (2008) Mat formation in *Saccharomyces cerevisiae* requires nutrient and pH gradients. Eukaryot Cell 7(1):122–130. https://doi.org/10.1128/ec.00310-06

Simpson MJ, Baker RE, McCue SW (2011) Models of collective cell spreading with variable cell aspect ratio: A motivation for degenerate diffusion models. Phys Rev E 83(2):021901. https://doi.org/10.1103/PhysRevE.83.021901

Sivashinsky GI (1977) Diffusion-thermal theory of cellular flames. Combust Sci Technol 15(3–4):137–146. https://doi.org/10.1080/00102207708946779

Tam A, Green J, Balasuriya S, Tek EL, Gardner JM, Sundstrom JF, Jiranek V, Binder BJ (2018) Nutrient-limited growth with non-linear cell diffusion as a mechanism for floral pattern formation in yeast biofilms. J Theor Biol 448:122–141. https://doi.org/10.1016/j.jtbi.2018.04.004

Tam A, Green J, Balasuriya S, Tek EL, Gardner JM, Sundstrom JF, Jiranek V, Binder BJ (2019) A thin-film extensional flow model for biofilm expansion by sliding motility. Proc Royal Soc A 475(2229):20190175. https://doi.org/10.1098/rspa.2019.0175

Tam A, Harding B, Green J, Balasuriya S, Binder BJ (2022) Thin-film lubrication model for biofilm expansion under strong adhesion. Phys Rev E 105(1):014408. https://doi.org/10.1103/PhysRevE.105.014408

Tek EL, Sundstrom JF, Gardner JM, Oliver SG, Jiranek V (2018) Evaluation of the ability of commercial wine yeasts to form biofilms (mats) and adhere to plastic: Implications for the microbiota of the winery environment. FEMS Microbiol Ecol 94(2):188. https://doi.org/10.1093/femsec/fix188

Tronnolone H, Tam A, Szenczi Z, Green J, Balasuriya S, Tek EL, Gardner JM, Sundstrom JF, Jiranek V, Oliver SG, Binder BJ (2018) Diffusion-limited growth of microbial colonies. Sci Rep 8:5992. https://doi.org/10.1038/s41598-018-23649-z

Váchová L, Palková Z (2005) Physiological regulation of yeast cell death in multicellular colonies is triggered by ammonia. J Cell Biol 169(5):711–717. https://doi.org/10.1083/jcb.200410064

Váchová L, Šťovíček V, Hlaváček O, Chernyavskiy O, Štěpánek L, Kubínová L, Palková Z (2011) Flo11p, drug efflux pumps, and the extracellular matrix cooperate to form biofilm yeast colonies. J Cell Biol 194(5):679–687. https://doi.org/10.1083/jcb.201103129

Wanner O, Gujer W (1986) A multispecies biofilm model. Biotechnol Bioeng 28(3):314–328. https://doi.org/10.1002/bit.260280304

Ward JP, King JR (2012) Thin-film modelling of biofilm growth and quorum sensing. J Eng Math 73(1):71–92. https://doi.org/10.1007/s10665-011-9490-4

Werner-Washburne M, Braun EL, Crawford ME, Peck VM (1996) Stationary phase in *Saccharomyces cerevisiae*. Mol Microbiol 19(6):1159–1166. https://doi.org/10.1111/j.1365-2958.1996.tb02461.x

Yang J, D'Onofrio A, Kalliadasis S, De Wit A (2002) Rayleigh-Taylor instability of reaction-diffusion acidity fronts. J Chem Phys 117(20):9395–9408. https://doi.org/10.1063/1.1516595

Publisher's Note Springer Nature remains neutral with regard to jurisdictional claims in published maps and institutional affiliations.

Authors and Affiliations

Daniel J. Netherwood[1] [iD] **· Alexander K. Y. Tam[2]** [iD] **·**
Campbell W. Gourlay[3] [iD] **· Tea Knežević[4]** [iD] **· Jennifer M. Gardner[4]** [iD] **·**
Vladimir Jiranek[5] [iD] **· Benjamin J. Binder[1]** [iD] **· J. Edward F. Green[1]**

✉ Vladimir Jiranek
  v.jiranek@soton.ac.uk

  Daniel J. Netherwood
  daniel.netherwood@adelaide.edu.au

  Alexander K. Y. Tam
  alex.tam@unisa.edu.au

  Campbell W. Gourlay
  c.w.gourlay@kent.ac.uk

  Tea Knežević
  tea.knezevic@adelaide.edu.au

  Jennifer M. Gardner
  jennie.gardner@adelaide.edu.au

  Benjamin J. Binder
  benjamin.binder@adelaide.edu.au

  J. Edward F. Green
  edward.green@adelaide.edu.au

[1] School of Computer and Mathematical Sciences, The University of Adelaide, North Terrace
     Campus, Adelaide 5000, SA, Australia

[2] UniSA STEM, The University of South Australia, Mawson Lakes Campus, Mawson Lakes 5095,
     SA, Australia

[3] Kent Fungal Group, School of Biosciences, The University of Kent, Canterbury CT2 9HY, Kent,
     United Kingdom

[4] Discipline of Wine Science, School of Agriculture, Food and Wine, The University of Adelaide,
     Waite Campus, Urrbrae 5064, SA, Australia

[5] School of Biological Sciences, The University of Southampton, Southampton SO17 1BJ, United
     Kingdom